



Communication

Enhancing Photocatalytic Hydrogen Production of g-C₃N₄ by Selective Deposition of Pt Cocatalyst

Yang Li ¹, Yue Lu ¹, Zhaoyu Ma ¹, Lianqing Dong ², Xiaofang Jia ¹ and Junying Zhang ^{1,*}¹ School of Physics, Beihang University, Beijing 100191, China; liyang1619125@buaa.edu.cn (Y.L.);

Luyue@buaa.edu.cn (Y.L.); 18338208022@163.com (Z.M.); jiaxiaofang@buaa.edu.cn (X.J.)

² Beijing Institute of Space Mechanics & Electricity, Beijing 100094, China; XPHDLQ@163.com

* Correspondence: zjy@buaa.edu.cn

Abstract: Graphitic carbon nitride (g-C₃N₄) has been widely studied as a photocatalyst for the splitting of water to produce hydrogen. In order to solve the problems of limited number of active sites and serious recombination rate of charge-carriers, noble metals are needed as cocatalysts. Here, we selectively anchored Pt nanoparticles (NPs) to specific nitrogen species on the surface of g-C₃N₄ via heat treatment in argon–hydrogen gas mixture, thus achieving g-C₃N₄ photocatalyst anchored by highly dispersed homogeneous Pt NPs with the co-existed metallic Pt⁰ and Pt²⁺ species. The synergistic effect of highly dispersed metallic Pt⁰ and Pt²⁺ species makes the catalyst exhibit excellent photocatalytic performance. Under the full-spectrum solar light irradiation, the photocatalytic hydrogen production rate of the photocatalyst is up to 18.67 mmol·g⁻¹·h⁻¹, which is 5.1 times of the catalyst prepared by non-selective deposition of Pt NPs.

Keywords: graphitic carbon nitride; platinum; selective deposition; photocatalytic hydrogen production



Citation: Li, Y.; Lu, Y.; Ma, Z.; Dong, L.; Jia, X.; Zhang, J. Enhancing Photocatalytic Hydrogen Production of g-C₃N₄ by Selective Deposition of Pt Cocatalyst. *Nanomaterials* **2021**, *11*, 3266. <https://doi.org/10.3390/nano11123266>

Academic Editor:
Detlef W. Bahnemann

Received: 27 October 2021
Accepted: 29 November 2021
Published: 30 November 2021

Publisher's Note: MDPI stays neutral with regard to jurisdictional claims in published maps and institutional affiliations.



Copyright: © 2021 by the authors. Licensee MDPI, Basel, Switzerland. This article is an open access article distributed under the terms and conditions of the Creative Commons Attribution (CC BY) license (<https://creativecommons.org/licenses/by/4.0/>).

1. Introduction

With the development of world economy and the increase of population, the demand for energy is increasing continually [1,2]. In order to reduce the dependence on non-renewable energy, it is very important to develop environmentally friendly alternative energy. In 1972, Fujishima and Honda creatively revealed the possibility for photocatalytic water splitting to generate hydrogen by TiO₂ photoelectrode [3]. Since then, investigating on the semiconductor photocatalyst have been carried out extensively [4–11]. Among the photocatalytic semiconductors studied, g-C₃N₄ has been considered as an ideal photocatalyst with moderate band gap (2.7 eV) and stable physical and chemical properties [12–19].

While g-C₃N₄ has the aforementioned superiority, the feature of low electrical conductivity and high recombination rate of charge-carriers limit its application [20–23]. To overcome these two barriers, noble metals are often used as cocatalysts to accelerate electron transfer to inhibit recombination and reduce redox overpotential at the active sites [24,25]. Nevertheless, noble metals are relatively expensive, so it is of importance to explore a more efficient method for dispersion of noble metals and their combination with g-C₃N₄ [26,27]. To pursue this goal, a large number of studies have been reported on the dispersion and binding of noble metals on g-C₃N₄ as cocatalysts [28–31]. Among them, Zhu et al. [31] found that the anchoring environment of noble metals on carbon nitride could be adjusted through chemical treatment. Wang et al. proposed that different types of nitrogen play different roles in bonding noble metals, which was confirmed by experiments and calculations. Among the nitrogen species involved, tri-coordination graphitized nitrogen (N-(C)₃) is considered to be beneficial to the nucleation and dispersion of noble metal NPs, while pyridine nitrogen (C-N=C) may play a role in the anchoring and dispersion of noble metal NPs [32]. This enlightens that we can selectively deposit Pt NPs on g-C₃N₄ by tuning the interaction of Pt with the different chemically-bonded nitrogen atoms, which will greatly influence the photocatalytic activity of g-C₃N₄.

In the present work, three deposition methods of Pt NPs were conducted based on the lattice sites of N atoms. For the first two conditions, Pt NPs were selectively deposited on N-(C)₃ and C-N=C of g-C₃N₄ by heat treatment in argon–hydrogen mixture and air, respectively. For the last case, Pt NPs were indiscriminately deposited on g-C₃N₄ by photoreduction method. The photocatalytic hydrogen production test indicated that the catalysts obtained by selectively depositing Pt on the N-(C)₃ site of g-C₃N₄ (named CNH-Pt) showed best photocatalytic performance. Under full-spectrum solar light irradiation, the photocatalytic hydrogen production rate of CNH-Pt is 622.3 and 5.1 times those of the pure g-C₃N₄ and the catalyst with undifferentiated Pt NPs deposition (CNP-Pt), respectively.

2. Materials and Methods

2.1. Materials

Urea (A.R. > 99%) and triethanolamine (A.R.) were purchased from Shanghai Aladdin Bio-Chem Technology Co., Ltd., Shanghai, China, and chloroplatinic acid hexahydrate (A.R. Pt ≥ 37.5%) was purchased from Shanghai Macklin Biochemical Co., Ltd., Shanghai, China. All reagents were used without further purification.

2.2. Preparation of Catalyst

Preparation of g-C₃N₄: g-C₃N₄ was synthesized according to the method reported in previous literature [33]. 10 g Urea was heated at 500 °C for 2 h in a muffle furnace with a ramp rate of 5 °C min⁻¹, then cooled naturally and ground to get milky powder.

Preparation of Pt-loaded g-C₃N₄:

Preparation of CNH-Pt (Pt NPs are selectively deposited on N-(C)₃): 300 mg g-C₃N₄ powder was dispersed in 20 mL deionized water and the solution was ultrasonically vibrated for 30 min. Then appropriate amount of H₂PtCl₆·6H₂O solution was added drop by drop and stirred for 30 min. Finally, the pale-yellow powder was obtained by freeze drying. 100 mg of dried pale-yellow powder was heated in a tubular furnace at 400 °C for 1 h in argon–hydrogen (90 vol%Ar-10 vol% H₂) atmosphere to obtain grey powder. The sample with 3 wt% Pt loading was named as CNH-Pt.

Preparation of CNA-Pt (Pt NPs are selectively deposited on C-N=C): Under the same conditions, the aforementioned pale-yellow powder was annealed in air atmosphere instead of argon–hydrogen atmosphere, and the sample with 3 wt% Pt loading was named as CNA-Pt.

Preparation of CNP-Pt (Pt NPs are deposited indiscriminately): Pt NPs were indiscriminately loaded onto g-C₃N₄ through photoreduction. One hundred milligrams of g-C₃N₄ was dispersed in 40 mL water and the solution was ultrasonically vibrated for 30 min. Then a certain amount of H₂PtCl₆·6H₂O solution with the designed nominal 3 wt% Pt was added, and the solution was stirred under the irradiation of a xenon lamp (300 W) for 1 h. Finally, the catalyst was obtained after freeze drying and named as CNP-Pt.

As the control group, the sample obtained by annealing of g-C₃N₄ in argon–hydrogen atmosphere without Pt was named as CNH, and the sample obtained by annealing of g-C₃N₄ in air without Pt was named as CNA. The annealing time, temperature and heating rate were consistent with CNH-Pt.

First-principles calculation methods and characterization and photocatalytic tests of the materials are detailed in Supporting Information.

3. Results and Discussion

The crystal structures of the samples can be depicted through the X-ray powder diffraction (XRD) pattern, as shown in Figure 1. Pure g-C₃N₄ shows two characteristic peaks located at around 13.2° and 27.4°, which are attributed to the in-plane ordering of tri-s-triazine units (indexed as (100)) and the interlayer stacking of conjugated aromatic systems (indexed as (002)), respectively [34]. CNH and CNA also show similar diffraction patterns, indicating that high temperature heat treatment does not destroy the crystal structure of g-C₃N₄ (Figure S1). The diffraction peaks at around 13.2° and 27.4° also appear

in the patterns of samples CNH-Pt, CNA-Pt, and CNP-Pt, indicating that g-C₃N₄ preserve its crystal structure with Pt NPs loaded into it. In addition, weak peaks at 39.7° have been detected in CNH-Pt, CNA-Pt, and CNP-Pt, which are diffraction peaks corresponding to Pt (111) crystal plane [31], which can be concluded that Pt NPs have been loaded onto g-C₃N₄ by three different methods. Among them, the diffraction peaks of CNH-Pt and CNA-Pt at 39.7° are obvious, which is due to the good crystallinity of Pt obtained by high temperature heat treatment. The diffraction peak of CNP-Pt at 39.7° is weaker, which may be because the photoreduction process is carried out at 10 °C, and the lower temperature makes part of Pt exist in amorphous form and has not been detected. In addition, inductively coupled plasma optical emission spectrometer (ICP-OES) results show that the actual Pt loads concentration of CNH-Pt, CNA-Pt, and CNP-Pt are all about 3 wt% (Table S1).

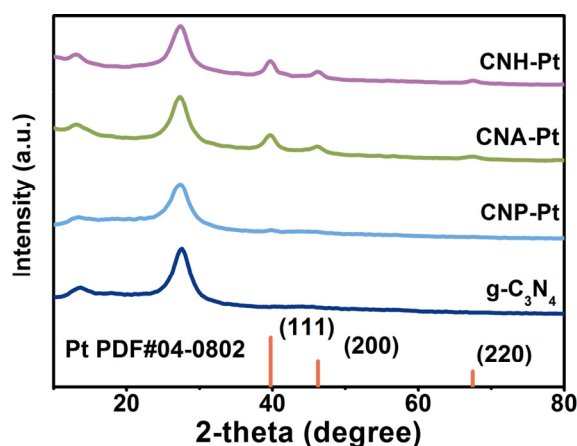


Figure 1. XRD patterns of the catalysts.

Transmission electron microscopy (TEM) images (Figure 2) show the microscopic morphology of g-C₃N₄ loaded with Pt NPs. As can be seen from Figure 2a,b, Pt NPs loaded on CNH-Pt have uniform sizes of about 2.5 nm and disperse evenly on the surface of g-C₃N₄. However, the size of Pt NPs on CNA-Pt varies from 1 nm to 13 nm (Figure 2c,d). The size of Pt NPs on CNP-Pt is similar to that on CNH-Pt (about 3.5 nm), but multiple Pt NPs accumulate into clusters, and each Pt particle does not exist independently (Figure 2e,f). HRTEM images of CNH-Pt, CNA-Pt, and CNP-Pt are shown in the insets of 2a, 2c and 2e, respectively. The Pt NPs lattice distances of CNH-Pt, CNA-Pt, and CNP-Pt are identical at 0.227 nm, corresponding to the (111) plane of metallic Pt [35], presenting a consistency with the XRD results. Meanwhile, it can be observed from the illustration of Figure 2e that some Pt NPs have poor crystallinity, which is consistent with the weak diffraction peak of CNP-Pt at 39.7° in the XRD pattern (Figure 1).

X-ray photoelectron spectroscopy (XPS) analysis was carried out to further study the binding of Pt NPs to g-C₃N₄. The N 1s spectrum is fitted with two peaks located at 398.7 eV and 400.4 eV (Figure 3a–c). A dominant peak at 398.7 eV corresponds to the N₂C in C–N=C groups [36,37], while weak peak at the high binding energy 400.4 eV is attributed to the N₃C in N–(C)₃ groups [38]. It is worth noting that the ideal g-C₃N₄ has only two functional groups, C–N=C and N–(C)₃, but the experimentally synthesized g-C₃N₄ often contains a small number of C–N–H functional groups. It can be seen from the fitting XPS of the three functional groups (Figure S2) that the content of C–N–H is very small. The C 1s spectrum can be divided into three peaks located at 284.8, 286.6, and 288.2 eV, which are assigned to the adventitious carbon, sp³ hybridized carbon (C–(N)₃) and N–C=N coordination in the framework of g-C₃N₄, respectively (Figure S3) [39,40]. After loading Pt NPs, the N 1s peak and C 1s peak of the samples do not change significantly, indicating that the loading of Pt NPs on g-C₃N₄ do not destroy its basic structure.

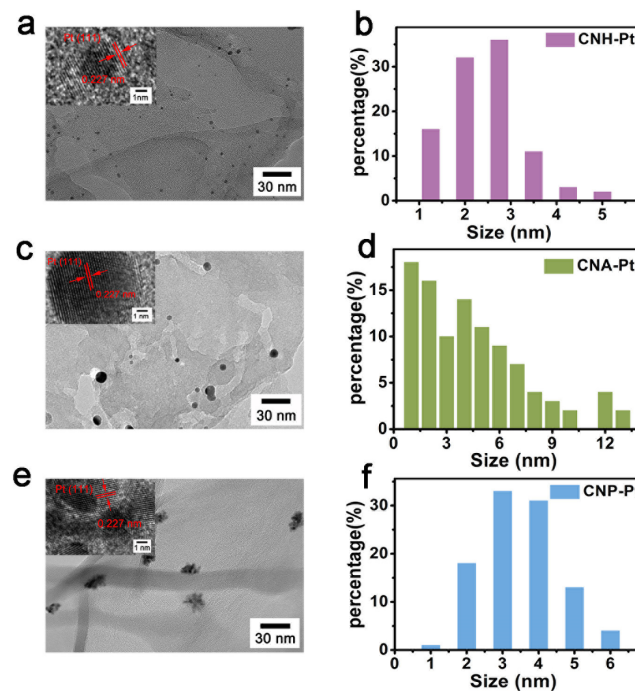


Figure 2. TEM images and Pt NPs size distribution of CNH-Pt (a,b), CNA-Pt (c,d), and CNP-Pt (e,f). Insets show HRTEM images of CNH-Pt (a), CNA-Pt (c), and CNP-Pt (e).

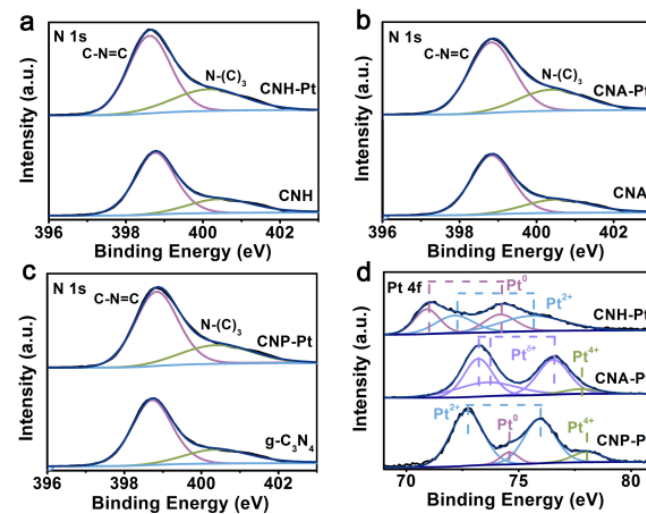


Figure 3. XPS spectra of N 1s of CNH-Pt and CNH (a), CNA-Pt and CNA (b), CNP-Pt, and g-C₃N₄ (c). (d) Pt 4f spectra of CNH-Pt, CNA-Pt, and CNP-Pt.

The Pt 4f spectra of CNH-Pt, CNA-Pt and CNP-Pt are shown in Figure 3d. The Pt 4f peak of CNH-Pt can be decomposed into four peaks, and the peaks located at 70.9 eV and 74.2 eV are attributed to metal Pt⁰, and peaks located at 72.2 eV and 75.7 eV are corresponding to Pt²⁺. Metal Pt⁰ can promote electron transport and separation, and Pt²⁺ species can suppress the hydrogen back reaction [41,42]. The coexistence of Pt⁰ and Pt²⁺ makes CNH-Pt possess better photocatalytic performance. The Pt 4f peaks of CNA-Pt can be divided to obtain the peaks of Pt^{δ+} ($2 < \delta < 4$) at 73.2 eV, 73.6 eV, and 76.5 eV, and a small amount of Pt⁴⁺ at 77.8 eV [37]. Owing to the reducing ability of air is too weak, Pt⁴⁺ in CNA-Pt can only be reduced to Pt^{δ+} even at high temperature. Similarly, the reducing ability of light is not strong enough to reduce all Pt⁴⁺ to a lower valence state, resulting in the existence of part of Pt⁴⁺ in CNP-Pt. The photocatalytic performance of CNA-Pt and CNP-Pt is mediocre due to the incomplete reduction of Pt⁴⁺ and the absence or small

amount of metal Pt^0 . Simultaneously, there are also Pt^{2+} peaks located at 72.7 eV and 75.9 eV and Pt^0 peaks located at 74.6 eV in CNP-Pt [41,42]. Comparing with CNP-Pt, the binding energy of Pt^{2+} and Pt^0 peaks of CNH-Pt is lower, indicating that Pt NPs in CNH-Pt can attract more electrons [31].

The surface contents of the two N species in different catalysts are depicted in Figure 4a–c, showing no significance difference between CNH, CNA and pure $\text{g-C}_3\text{N}_4$. However, after loading Pt NPs with three different methods, the surface content of the two N species alters significantly, which is caused by Pt NPs selective anchoring on the different N species [31]. Figure 4d–f shows the variation in the proportions of the two N species on the catalyst surface before and after loading Pt NPs. Compared with CNH, the ratio of N-(C)_3 in CNH-Pt decrease from 29.6% to 20.0%, indicating that Pt NPs in CNH-Pt are mainly anchored on N-(C)_3 . N-(C)_3 is believed to play an important role in the nucleation and dispersion of noble metal particles, and the Pt particles bound to it have high adsorption energy [32,43]. Therefore, it is less likely to attract a large number of Pt atoms to form large particles, which also explains the high dispersity and relatively small size of Pt NPs in CNH-Pt. The C-N=C decrease from 70.4% in CNA to 66.7% in CNA-Pt, indicating that Pt NPs in CNA-Pt are mainly supported by C-N=C . C-N=C can be used as an anchor point, and the Pt attached to it has a lower adsorption energy [32,43]. It is easier for Pt atoms to coalesce into larger particles, which is consistent with TEM observations of larger Pt NPs in CNA-Pt (Figure 2c). However, comparing with pure $\text{g-C}_3\text{N}_4$, the proportion of N species in CNP-Pt is basically maintained. Pt NPs in CNP-Pt are not selectively connected with N species, resulting in a large number of particles agglomerated together without being dispersed. From the fitting results of the N 1s spectra using three functional groups, the change of Pt deposition to ratio of N-(C)_3 and C-N=C follows the same trend with the results using two functional groups, and the C-N-H content hardly changes before and after loading Pt (Figure S4). Therefore, only C-N=C and N-(C)_3 will be discussed below.

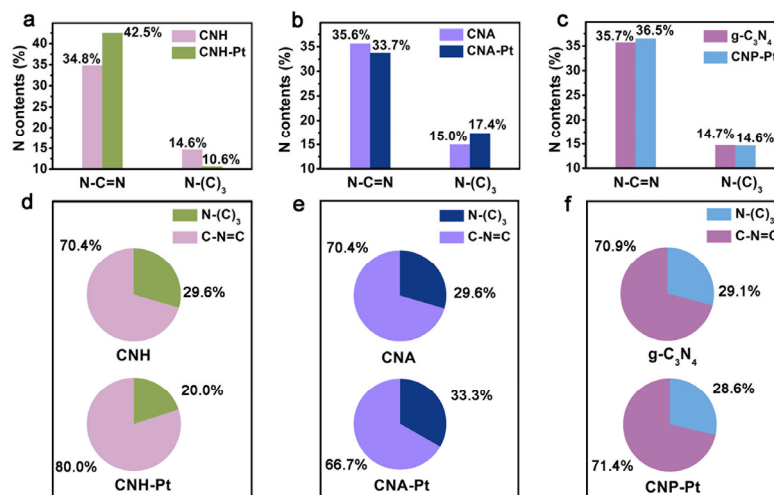


Figure 4. The surface N species content of CNH-Pt and CNH (a), CNA-Pt and CNA (b), CNP-Pt and $\text{g-C}_3\text{N}_4$ (c). The ratio of N-(C)_3 and C-N=C before and after Pt loading of CNH (d), CNA (e), and $\text{g-C}_3\text{N}_4$ (f).

In order to further confirm the selective deposition of Pt NPs on different types of nitrogen in different atmospheres, the adsorption energies of C-N=C and N-(C)_3 to hydrogen were calculated using first-principles calculations. As shown in Figure 5, the adsorption energy of C-N=C for hydrogen (-0.87 eV) is much lower than that of N-(C)_3 (-0.04 eV). Meanwhile, the adsorption of hydrogen at the C-N=C site causes obvious structural distortion of $\text{g-C}_3\text{N}_4$. As C-N=C is easier to adsorb hydrogen, more Pt NPs in CNH-Pt obtained by heat treatment in argon–hydrogen atmosphere will be adsorbed by N-(C)_3 . The adsorption capacity of C-N=C to Pt atoms is stronger than that of N-(C)_3 [43],

so Pt NPs in CNA-Pt obtained by air annealing without the influence of hydrogen are more likely to deposit on the position of C-N=C, which is consistent with XPS test results, confirming the hypothesis of selective deposition of Pt NPs.

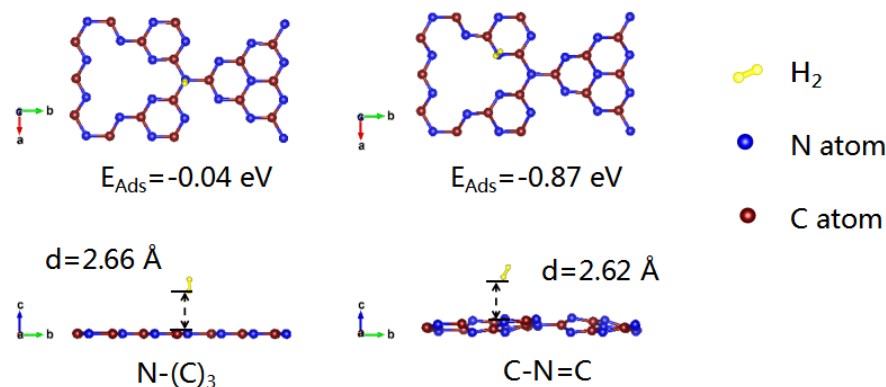


Figure 5. Adsorption energy of hydrogen on N-(C)₃ and C-N=C.

Electrochemical impedance spectroscopy (EIS) and photoluminescence (PL) was used to verify the electrical conductivity and the recombination rate of charge-carriers. Semicircular Nyquist plots of CNH-Pt show obviously reduced diameter (Figure 6a), indicating its smaller charge carrier transport resistance and higher separation efficiency of electrons and holes [42,44,45]. The PL peak of CNH-Pt at 470 nm is significantly lower than that of g-C₃N₄ (Figure S5), indicating more effective separation of photoexcited electrons and holes in CNH-Pt [46]. The results of EIS and PL show that Pt loading reduces the charge-carriers recombination rate of the material.

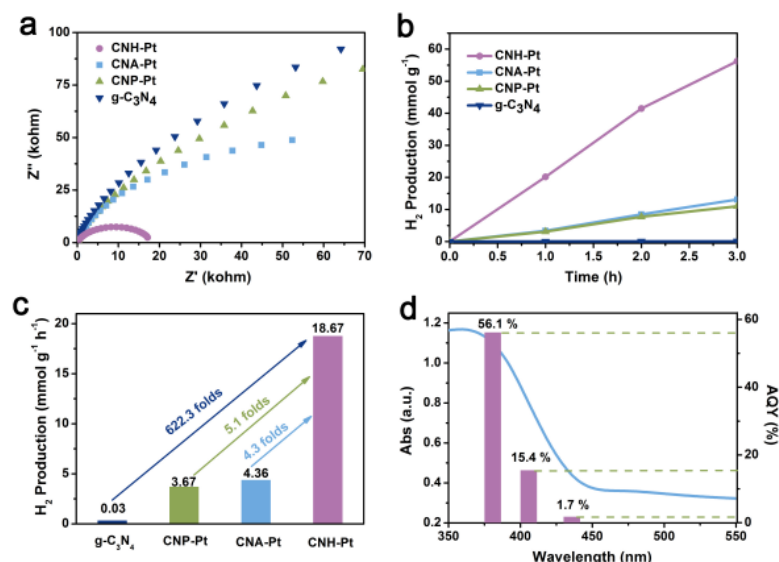


Figure 6. EIS Nyquist plots (a), time course of hydrogen evolution over 3 h (b) and hydrogen production rates (c) of CNH-Pt, CNA-Pt, CNP-Pt, and g-C₃N₄. (d) Wavelength-dependent AQY and absorption spectrum of CNH-Pt.

The photocatalytic hydrogen production performance of the catalyst was tested under full-spectrum simulated solar-light. Figure 6b shows the accumulation of hydrogen production over time within 3 h. The hydrogen production of pure g-C₃N₄ is very small, but the hydrogen production of the catalysts supported by Pt NPs all increases. Figure 6c shows the average hydrogen production rate of the catalysts, among which the average hydrogen production rate of CNH-Pt is up to 18.67 mmol·g⁻¹·h⁻¹, 622.3 times the 0.03 mmol·g⁻¹·h⁻¹ of pure g-C₃N₄. Comparing with pure g-C₃N₄, the average hy-

drogen production rates of CNP-Pt and CNA-Pt are also greatly improved, reaching $3.67 \text{ mmol}\cdot\text{g}^{-1}\cdot\text{h}^{-1}$ and $4.36 \text{ mmol}\cdot\text{g}^{-1}\cdot\text{h}^{-1}$, respectively, but far lower than that of CNH-Pt. The excellent photocatalytic performance of CNH-Pt may be attributed to the following two aspects: (i) Pt NPs with small size and high dispersion provide sufficient reaction sites for decomposition of aquatic hydrogen; (ii) The synergistic effect of Pt^0 and Pt^{2+} promotes charge separation and transfer while inhibiting the unexpected hydrogen reverse reaction [42]. Cyclic stability test is shown in Figure S6, where the hydrogen production activity of CNH-Pt decreases with reaction time, possibly due to Pt leaching during the reaction. After 9 h of reaction, the samples were collected for ICP test, in which the Pt content was reduced to about 1 wt%. The wavelength-dependent apparent quantum yield (AQY) of CNH-Pt photocatalyst matches the light absorption spectra, and the AQY is estimated to be about 56.1% at 380 nm, 15.4% at 405 nm and 1.7% at 435 nm, respectively (Figure 6d). The AQY of CNH-Pt is better at 380 nm, which is consistent with its absorption capacity of light. The hydrogen production efficiency of CNH-Pt can reach $4.40 \text{ mmol}\cdot\text{g}^{-1}\cdot\text{h}^{-1}$, even under the very weak light intensity of 380 nm monochromatic light (obtained with 380 nm band pass filter) (Figure S7). Although CNH-Pt has slightly enhanced absorption of light above 400 nm compared with original $\text{g}\text{-C}_3\text{N}_4$, it still absorbs ultraviolet light mainly (Figure S8). Because ultraviolet light only accounts for about 5% of sunlight, the absorption spectrum of the sample should be broadened in the follow-up work to enhance the utilization of the solar light.

Table 1 shows the main concerns and the photocatalytic activity of hydrogen production of previous works on the same topic. In the previous work, there is no study on the effect of selective deposition of Pt on the activity of photocatalytic hydrogen production, and the catalyst prepared in this work has a competitive advantage in the activity of hydrogen production, which can provide reference for the subsequent work in related fields.

Table 1. The main concerns and hydrogen evolution data of previous work.

Research Highlights	Pt Amount (wt%)	H ₂ Evolution Rate	Light Source	Sacrificial Agent	Ref.
Effect of Pt Shape	1	$588 \mu\text{mol g}^{-1} \text{h}^{-1}$	350 W Xe lamp (>400 nm)	10% TEOA	[25]
Order of addition of sacrificial agent	1	$4210 \mu\text{mol g}^{-1} \text{h}^{-1}$	350 W Xe lamp	10% TEOA	[27]
Reactive metal-support interaction to stabilize Pt single atoms	1.72	$3020 \mu\text{mol g}^{-1} \text{h}^{-1}$	300 W Xe lamp (>420 nm)	10% TEOA	[36]
A bridging Pt-N bond boosted electron transfer	1.24	$11,472 \mu\text{mol g}^{-1} \text{h}^{-1}$	300 W Xe lamp	20% TEOA	[37]
Effect of Pt size	3	$473.82 \mu\text{mol mg}^{-1}$ Pt for 4 h	>420 nm	10% methanol	[38]
Anchoring $\text{Pt}^{2+}/\text{Pt}^0$ on $\text{g}\text{-C}_3\text{N}_4$ nitrogen vacancies	0.5	$2626 \mu\text{mol g}^{-1} \text{h}^{-1}$	300 W Xe lamp (>420 nm)	15% TEOA	[42]
Selective deposition of Pt	3	$18,670 \mu\text{mol g}^{-1} \text{h}^{-1}$	300 W Xe lamp (AM1.5)	25% TEOA	This work

4. Conclusions

In conclusion, in this paper, Pt NPs composed of Pt^0 and Pt^{2+} were selectively deposited on tri-coordination graphitized nitrogen of $\text{g}\text{-C}_3\text{N}_4$ by heat-treatment in argon-hydrogen atmosphere, and thus photocatalyst with Pt cocatalyst of uniform size and good dispersity was achieved. From theoretical calculation, it is found that hydrogen is more easily adsorbed on pyridine nitrogen, so that more Pt NPs can be deposited on tri-coordination graphitized nitrogen. The internal mechanism of selective deposition of Pt NPs by heat-treatment in different atmospheres is clarified. The highly-dispersed Pt NPs promote the separation of electrons and holes and the transfer of electrons to hydrogen ion. The photocatalytic hydrogen productivity of this photocatalyst reaches $18.67 \text{ mmol}\cdot\text{g}^{-1}\cdot\text{h}^{-1}$, which is 4.3 times that of the photocatalyst when Pt aggregated nanoparticles are selectively

deposited on pyridine nitrogen of g-C₃N₄, and 5.1 times that of the photocatalyst when Pt NPs of inhomogeneous size are indifferently deposited on g-C₃N₄. These results indicate that selective deposition of Pt cocatalyst on the surface of g-C₃N₄ will affect the size and distribution of Pt NPs, and then greatly influence the photocatalytic activity of the catalyst. The present work provides a reference for further study of anchoring noble metal cocatalyst on the semiconductor surface to improve the photocatalytic performance.

Supplementary Materials: The following are available online at <https://www.mdpi.com/article/10.3390/nano11123266/s1>, Table S1: The theoretical and actual loading Pt (wt%) of catalyst; Figure S1. XRD patterns of CNH, CNA and g-C₃N₄; Figure S2. XPS spectra of N 1s of catalysts with three functional groups; Figure S3. XPS spectra of C 1s of CNH-Pt and CNH (a), CNA-Pt and CNA (b), CNP-Pt and g-C₃N₄ (c); Figure S4. The ratio of N-(C)₃, C-N=C and C-N-H before and after Pt loading on the catalysts; Figure S5. PL spectra of g-C₃N₄ and CNH-Pt; Figure S6 Recycle ability of CNH-Pt for the photocatalytic H₂ evolution; Figure S7. Time course of hydrogen evolution over 3 h of CNH-Pt under 380 nm monochromatic light (a), the transmission spectrum of the 380nm band-pass filter (b); Figure S8. UV-vis absorption spectra of CNH-Pt, CNA-Pt, CNP-Pt and g-C₃N₄.

Author Contributions: Y.L. (Yang Li) finished the experiment and completed writing the paper. Y.L. (Yue Lu) completed the data analysis. Z.M. designed the research scheme. L.D. modified and verified the draft. X.J. undertook the work of first principles calculation. J.Z. designed the research scheme and finished the paper submission. All authors have read and agreed to the published version of the manuscript.

Funding: This project is financially supported by the National Natural Science Foundation of China (Grant No. 51972010).

Data Availability Statement: The data presented in this study are available on request from the corresponding author.

Acknowledgments: We are grateful for the financial support from the National Natural Science Foundation of China.

Conflicts of Interest: We declare no conflict of interest.

References

1. Wu, X.; Zhang, H.; Dong, J.; Qiu, M.; Kong, J.; Zhang, Y.; Ye, J. Surface Step Decoration of Isolated Atom as Electron Pumping: Atomic-Level Insights into Visible-Light Hydrogen Evolution. *Nano Energy* **2018**, *45*, 109–117. [[CrossRef](#)]
2. Liu, G.; Yan, S.; Shi, L.; Yao, L. The improvement of photocatalysis H₂ evolution over g-C₃N₄ with Na and cyano-group co-modification. *Front. Chem.* **2019**, *7*, 639. [[CrossRef](#)] [[PubMed](#)]
3. Fujishima, A.; Honda, K. Electrochemical Photolysis of Water at a Semiconductor Electrode. *Nature* **1972**, *238*, 37–38. [[CrossRef](#)]
4. Zhu, M.; Cai, X.; Fujitsuka, M.; Zhang, J.; Majima, T. Au/La₂Ti₂O₇ Nanostructures Sensitized with Black Phosphorus for Plasmon-Enhanced Photocatalytic Hydrogen Production in Visible and Near-Infrared Light. *Angew. Chem. Int. Ed.* **2017**, *56*, 2064–2068. [[CrossRef](#)] [[PubMed](#)]
5. Hisatomi, T.; Kubota, J.; Domen, K. Recent Advances in Semiconductors for Photocatalytic and Photoelectrochemical Water Splitting. *Chem. Soc. Rev.* **2014**, *43*, 7520–7535. [[CrossRef](#)]
6. Shi, Y.; Ma, J.; Chen, Y.; Qian, Y.; Xu, B.; Chu, W.; An, D. Recent Progress of Silver-Containing Photocatalysts for Water Disinfection under Visible Light Irradiation: A Review. *Sci. Total. Environ.* **2021**, *804*, 150024. [[CrossRef](#)]
7. Zhang, D.; He, W.; Ye, J.; Gao, X.; Wang, D.; Song, J. Polymeric Carbon Nitride-Derived Photocatalysts for Water Splitting and Nitrogen Fixation. *Small* **2021**, *17*, 2005149. [[CrossRef](#)]
8. Dong, B.; Cui, J.; Gao, Y.; Qi, Y.; Zhang, F.; Li, C. Heterostructure of 1D Ta₃N₅ Nanorod/BaTaO₂N Nanoparticle Fabricated by a One-Step Ammonia Thermal Route for Remarkably Promoted Solar Hydrogen Production. *Adv. Mater.* **2019**, *31*, 1808185. [[CrossRef](#)]
9. Sun, S.; Zhang, Y.C.; Shen, G.; Wang, Y.; Liu, X.; Duan, Z.; Pan, L.; Zhang, X.; Zou, J. Photoinduced Composite of Pt Decorated Ni (OH)₂ as Strongly Synergetic Cocatalyst to Boost H₂O Activation for Photocatalytic Overall Water Splitting. *Appl. Catal. B Environ.* **2019**, *243*, 253–261. [[CrossRef](#)]
10. Bakbolat, B.; Daulbayev, C.; Sultanov, F.; Beissenov, R.; Umirzakov, A.; Mereke, A.; Bekbaev, A.; Chuprakov, I. Recent developments of TiO₂-based photocatalysis in the hydrogen evolution and photodegradation: A review. *Nanomaterials* **2020**, *10*, 1790. [[CrossRef](#)] [[PubMed](#)]
11. Cai, X.; Zhang, J.; Fujitsuka, M.; Majima, T. Graphitic-C₃N₄ Hybridized N-Doped la₂ti₂o₇ Two-Dimensional Layered Composites as Efficient Visible-Light-Driven Photocatalyst. *Appl. Catal. B Environ.* **2017**, *202*, 191–198. [[CrossRef](#)]

12. Praus, P.; Smýkalová, A.; Foniok, K.; Velíšek, P.; Cvejn, D.; Žádný, J.; Storch, J. Post-Synthetic Derivatization of Graphitic Carbon Nitride with Methanesulfonyl Chloride: Synthesis, Characterization and Photocatalysis. *Nanomaterials* **2020**, *10*, 193. [[CrossRef](#)] [[PubMed](#)]
13. Han, Q.; Wang, B.; Gao, J.; Cheng, Z.; Zhao, Y.; Zhang, Z.; Qu, L. Atomically Thin Mesoporous Nanomesh of Graphitic C₃N₄ for High-Efficiency Photocatalytic Hydrogen Evolution. *ACS Nano* **2016**, *10*, 2745–2751. [[CrossRef](#)] [[PubMed](#)]
14. Kong, L.; Ji, Y.; Dang, Z.; Yan, J.; Li, P.; Li, Y.; Liu, S. g-C₃N₄ Loading Black Phosphorus Quantum Dot for Efficient and Stable Photocatalytic H₂ Generation Under Visible Light. *Adv. Funct. Mater.* **2018**, *28*, 1800668. [[CrossRef](#)]
15. Wu, M.; Gong, Y.; Nie, T.; Zhang, J.; Wang, R.; Wang, H.; He, B. Template-Free Synthesis of Nanocage-Like g-C₃N₄ with High Surface Area and Nitrogen Defects for Enhanced Photocatalytic H₂ Activity. *J. Mater. Chem. A* **2019**, *7*, 5324–5332. [[CrossRef](#)]
16. Xu, H.; Xiao, R.; Huang, J.; Jiang, Y.; Zhao, C.; Yang, X. In Situ Construction of Protonated g-C₃N₄/Ti₃C₂ MXene Schottky Heterojunctions for Efficient Photocatalytic Hydrogen Production. *Chin. J. Catal.* **2021**, *42*, 107–114. [[CrossRef](#)]
17. Sun, X.; Zhang, F.; Kong, C. Porous g-C₃N₄/WO₃ Photocatalyst Prepared by Simple Calcination for Efficient Hydrogen Generation under Visible Light. *Colloids. Surf. A Physicochem. Eng. Aspects* **2020**, *594*, 124653. [[CrossRef](#)]
18. Jin, Z.; Zhang, L. Performance of Ni-Cu bimetallic co-catalyst g-C₃N₄ nanosheets for improving hydrogen evolution. *J. Mater. Sci. Technol.* **2020**, *49*, 144–156. [[CrossRef](#)]
19. Li, Y.; Lu, Y.; Wang, Y.; Dong, L.; Chao, M.; Sun, J.; Zhao, Z.; Zhang, J. One-Step Synthesis of High Photocatalytic Graphitic Carbon Nitride Porous Nanosheets. *Nanotechnology* **2020**, *31*, 464001. [[CrossRef](#)]
20. Zhu, M.; Kim, S.; Mao, L.; Fujitsuka, M.; Zhang, J.; Wang, X.; Majima, T. Metal-Free Photocatalyst for H₂ Evolution in Visible to Near-Infrared Region: Black Phosphorus/Graphitic Carbon Nitride. *J. Am. Chem. Soc.* **2017**, *139*, 13234–13242. [[CrossRef](#)]
21. Xing, W.; Tu, W.; Han, Z.; Hu, Y.; Meng, Q.; Chen, G. Template-Induced High-Crystalline g-C₃N₄ Nanosheets for Enhanced Photocatalytic H₂ Evolution. *ACS Energy Lett.* **2018**, *3*, 514–519. [[CrossRef](#)]
22. Ge, L.; Zuo, F.; Liu, J.; Ma, Q.; Wang, C.; Sun, D.; Bartels, L.; Feng, P. Synthesis and Efficient Visible Light Photocatalytic Hydrogen Evolution of Polymeric g-C₃N₄ Coupled with CdS Quantum Dots. *J. Phys. Chem. C* **2012**, *116*, 13708–13714. [[CrossRef](#)]
23. Güy, N. Directional Transfer of Photocarriers on CdS/g-C₃N₄ Heterojunction Modified with Pd as a Cocatalyst for Synergistically Enhanced Photocatalytic Hydrogen Production. *Appl. Surf. Sci.* **2020**, *522*, 146442. [[CrossRef](#)]
24. Zhang, P.; Wang, T.; Zeng, H. Design of Cu-Cu₂O/g-C₃N₄ Nanocomponent Photocatalysts for Hydrogen Evolution under Visible Light Irradiation Using Water-Soluble Erythrosin B dye Sensitization. *Appl. Surf. Sci.* **2017**, *391*, 404–414. [[CrossRef](#)]
25. Cao, S.; Jiang, J.; Zhu, B.; Yu, J. Shape-Dependent Photocatalytic Hydrogen Evolution Activity over a Pt Nanoparticle Coupled g-C₃N₄ Photocatalyst. *Phys. Chem. Chem. Phys.* **2016**, *18*, 19457–19463. [[CrossRef](#)]
26. Zhang, L.; Long, R.; Zhang, Y.; Duan, D.; Xiong, Y.; Zhang, Y.; Bi, Y. Direct Observation of Dynamic Bond Evolution in Single-Atom Pt/C₃N₄ Catalysts. *Angew. Chem. Int. Ed.* **2020**, *59*, 6224–6229. [[CrossRef](#)] [[PubMed](#)]
27. Liu, M.; Xia, P.; Zhang, L.; Cheng, B.; Yu, J. Enhanced Photocatalytic H₂-Production Activity of g-C₃N₄ Nanosheets via Optimal Photodeposition of Pt as Cocatalyst. *ACS Sustain. Chem. Eng.* **2018**, *6*, 10472–10480. [[CrossRef](#)]
28. Li, W.; Wang, D.; Zhang, Y.; Tao, L.; Wang, T.; Zou, Y.; Wang, Y.; Chen, R.; Wang, S. Defect Engineering for Fuel-Cell Electrocatalysts. *Adv. Mater.* **2020**, *32*, 1907879. [[CrossRef](#)]
29. Tiwari, J.; Sultan, S.; Myung, C.; Yoon, T.; Li, N.; Ha, M.; Harzandi, A.; Park, H.; Kim, D.; Chandrasekaran, S.; et al. Multi-component Electrocatalyst with Ultralow Pt Loading and High Hydrogen Evolution Activity. *Nat. Energy* **2018**, *3*, 773–782. [[CrossRef](#)]
30. Sultan, S.; Tiwari, J.; Singh, A.; Zhumagali, S.; Ha, M.; Myung, C.; Thangavel, P.; Kim, K. Single Atoms and Clusters Based Nanomaterials for Hydrogen Evolution, Oxygen Evolution Reactions, and Full Water Splitting. *Adv. Energy Mater.* **2019**, *9*, 1900624. [[CrossRef](#)]
31. Li, J.; Zahid, M.; Sun, W.; Tian, X.; Zhu, Y. Synthesis of Pt Supported on Mesoporous g-C₃N₄ Modified by Ammonium Chloride and Its Efficiently Selective Hydrogenation of Furfural to Furfuryl Alcohol. *Appl. Surf. Sci.* **2020**, *528*, 146983. [[CrossRef](#)]
32. Mao, S.; Wang, C.; Wang, Y. The Chemical Nature of N Doping on N Doped Carbon Supported Noble METAL catalysts. *J. Catal.* **2019**, *375*, 456–465. [[CrossRef](#)]
33. Martin, D.; Qiu, K.; Shevlin, S.; Handoko, A.; Chen, X.; Guo, Z.; Tang, J. Highly Efficient Photocatalytic H₂ Evolution from Water Using Visible Light and Structure-Controlled Graphitic Carbon Nitride. *Angew. Chem. Int. Ed.* **2014**, *53*, 9240–9245. [[CrossRef](#)] [[PubMed](#)]
34. Guo, H.; Zhang, J.; Ma, L.; Chavez, J.; Yin, L.; Gao, H.; Tang, Z.; Chen, W. A Non-Rare-Earth Ions Self-Activated White Emitting Phosphor Under Single Excitation. *Adv. Funct. Mater.* **2015**, *25*, 6833–6838. [[CrossRef](#)]
35. Shiraiishi, Y.; Kofuji, Y.; Kanazawa, S.; Sakamoto, H.; Ichikawa, S.; Tanaka, S.; Hirai, T. Platinum Nanoparticles Strongly Associated with Graphitic Carbon Nitride as Efficient Co-catalysts for Photocatalytic Hydrogen Evolution under Visible Light. *Chem. Commun.* **2014**, *50*, 15255–15258. [[CrossRef](#)] [[PubMed](#)]
36. Zhou, P.; Lv, F.; Li, N.; Zhang, Y.; Mu, Z.; Tang, Y.; Lai, J.; Chao, Y.; Luo, M.; Lin, F.; et al. Strengthening Reactive Metal-Support Interaction to Stabilize High-Density Pt Single Atoms on Electron-Deficient g-C₃N₄ for Boosting Photocatalytic H₂ Production. *Nano Energy* **2019**, *56*, 127–137. [[CrossRef](#)]
37. Hu, Y.; Qu, Y.; Zhou, Y.; Wang, Z.; Wang, H.; Yang, B.; Yu, Z.; Wu, Y. Single Pt Atom-Anchored C₃N₄: A Bridging Pt-N Bond Boosted Electron Transfer for Highly Efficient Photocatalytic H₂ Generation. *Chem. Eng. J.* **2021**, *412*, 128749. [[CrossRef](#)]

38. Zhu, Y.; Wang, T.; Xu, T.; Li, Y.; Wang, C. Size Effect of Pt Co-catalyst on Photocatalytic Efficiency of g-C₃N₄ for Hydrogen Evolution. *Appl. Surf. Sci.* **2019**, *464*, 36–42. [[CrossRef](#)]
39. Wang, X.; Zhou, C.; Shi, R.; Liu, Q.; Waterhouse, G.; Wu, L.; Tung, C.; Zhang, T. Supramolecular Precursor Strategy for the Synthesis of Holey Graphitic Carbon Nitride Nanotubes with Enhanced Photocatalytic Hydrogen Evolution Performance. *Nano Res.* **2019**, *12*, 2385–2389. [[CrossRef](#)]
40. Dong, F.; Zhao, Z.; Xiong, T.; Ni, Z.; Zhang, W.; Sun, Y.; Ho, W. In Situ Construction of g-C₃N₄/g-C₃N₄ Metal-Free Heterojunction for Enhanced Visible-Light Photocatalysis. *ACS Appl. Mater. Interfaces* **2013**, *5*, 11392–11401. [[CrossRef](#)]
41. Ding, J.; Sun, X.; Wang, Q.; Li, D.; Li, X.; Li, X.; Cheng, L.; Zhang, X.; Tian, X.; Ostrikov, K. Plasma Synthesis of Pt/g-C₃N₄ Photocatalysts with Enhanced Photocatalytic Hydrogen Generation. *J. Alloys Compd.* **2021**, *873*, 159871. [[CrossRef](#)]
42. Xing, W.; Tu, W.; Ou, M.; Wu, S.; Yin, S.; Wang, H.; Chen, G.; Xu, R. Anchoring Active Pt²⁺/Pt⁰ Hybrid Nanodots on g-C₃N₄ Nitrogen Vacancies for Photocatalytic H₂ Evolution. *ChemSusChem* **2019**, *12*, 2029–2034. [[CrossRef](#)] [[PubMed](#)]
43. Muhich, C.; Westcott, J., IV; Morris, T.; Weimer, W.; Musgrave, C. The Effect of N and B Doping on Graphene and the Adsorption and Migration Behavior of Pt Atoms. *J. Phys. Chem. C* **2013**, *117*, 10523–10535. [[CrossRef](#)]
44. Wu, J.; Ji, X.; Yuan, X.; Zhao, Z.; Li, Y.; Wen, B.; Zhang, H.; Yu, D.; Zhao, Y.; Tian, Y. Regulating Polymerization in Graphitic Carbon Nitride to Improve Photocatalytic Activity. *Chem. Mater* **2019**, *31*, 9188. [[CrossRef](#)]
45. Ran, J.; Ma, T.; Gao, G.; Du, X.; Qiao, S. Porous P-Doped Graphitic Carbon Nitride Nanosheets for Synergistically Enhanced Visible-Light Photocatalytic H₂ Production. *Energy Environ. Sci.* **2015**, *8*, 3708–3717. [[CrossRef](#)]
46. Wu, C.; Xue, S.; Qin, Z.; Nazari, M.; Yang, G.; Yue, S.; Tong, T.; Ghasemi, H.; Hernandez, F.C.R.; Xue, S.; et al. Making g-C₃N₄ Ultra-Thin Nanosheets Active for Photocatalytic Overall Water Splitting. *Appl. Catal. B Environ.* **2021**, *282*, 119557. [[CrossRef](#)]